THE JOURNAL OF PHYSICAL CHEMISTRY C

C: Plasmonics; Optical, Magnetic, and Hybrid Materials

Largest Enhancement of Broadband Near-Infrared Emission of Ni in Transparent Nano-Glass Ceramics: Using Nd as Sensitizer and Yb as Energy Transfer Bridge

Yindong Zhang, Xiaobo Li, Zhiqiang Lai, Runan Zhang, Elfed Lewis, Asrul Izam Azmi, Zhigang Gao, Xiaosong Lu, Yushi Chu, Yanlei Liu, Quan Chai, Shiyu Sun, Jing Ren, and Jianzhong Zhang

J. Phys. Chem. C, **Just Accepted Manuscript** • DOI: 10.1021/acs.jpcc.9b00359 • Publication Date (Web): 29 Mar 2019

Largest Enhancement of Broadband Near-Infrared Emission of Ni^{2+} in Transparent Nano-Glass Ceramics: Using Nd^{3+} as Sensitizer and Yb^{3+} as Energy Transfer Bridge

Yindong Zhang [1], Xiaobo Li [1], Zhiqiang Lai [1], Runan Zhang [1], Elfed Lewis [2], Asrul Izam Azmi [1], Zhigang Gao [1], Xiaosong Lu [1], Yushi Chu [1], Yanlei Liu [1], Quan Chai [1], Shiyu Sun [3], Jing Ren [1,], and Jianzhong Zhang [1,*]*

Corresponding author: ren.jing@hrbeu.edu.cn (J. Ren), zhangjianzhong@hrbeu.edu.cn (J. Zhang)

[1] Key Laboratory of In-fiber Integrated Optics, Ministry Education of China, Harbin Engineering University, Harbin 150001, China

[2] Optical Fibre Sensors Research Centre, Department of Electronic and Computer Engineering, University of Limerick, Limerick, Ireland

[3] Key Laboratory of Materials for High Power Laser, Shanghai Institute of Optics and Fine Mechanics, CAS, Shanghai 201800, China

ABSTRACT: An ultrabroadband near-infrared (NIR) emission of Ni^{2+} is demonstrated in a highly transparent nano-glass ceramic (nano-GC) containing Ga_2O_3 nanocrystals with 808 nm excitation of Nd^{3+}. It is also shown that by adding Yb^{3+} as an energy transfer (ET) bridge, the Ni^{2+} emission could be substantially enhanced. The dopant distribution was studied using advanced analytical transmission electron microscopy. This, together with optical transmission measurements, steady-state and time-resolved emission spectra, is utilized to understand the underlying ET mechanisms between Nd^{3+}, Yb^{3+}, and Ni^{2+}. The feasibility of this device as a viable source is demonstrated using dual-laser pumping at 808 and 980 nm for the greatest Ni^{2+} emission enhancement reported to date. The $Nd^{3+}/Yb^{3+}/Ni^{2+}$ triply doped nano-GC offers a promising gain medium for broadband and tunable NIR fiber amplifiers.

1. Introduction

Transition metal (TM) ions (e.g., V^{3+}, Cr^{4+}, Ni^{2+} etc.) doped bulk and nano-crystals (NCs) have attracted intense recent attention because of their broadband near-infrared (NIR, 1000-1700 nm) photoluminescence (PL),[1-3] showing considerable potential for a variety of technologies including optical fiber communications, bioimaging and phototherapy etc. Gallium oxide (Ga_2O_3), appears to be an excellent host material due to its highly suitable ligand field environments for TM dopants. For example, green and red emissions have been demonstrated by incorporating Mn^{2+} and Cr^{3+} ions in Ga_2O_3 by substitution for the tetrahedrally and octahedrally

coordinated Ga^{3+} sites, respectively.[4] In recent years, nanostructured glass-ceramics (nano-GCs) containing Ga_2O_3 NCs have become a strong competitor to their crystalline counterparts thanks to attributes such as robustness, favorable chemical durability, ease of large-scale production and complex shaping (e.g., optical fibers).[5] Since nickel has a highly stable valence state (Ni^{2+}) among the studied TM ions, Ni^{2+} doped nano-GCs containing Ga_2O_3 NCs have proved to be a very promising candidate for tunable NIR light sources.[6-8]

However, a looming challenge exists as Ni^{2+} often suffers from much weaker (by two orders of magnitude) PL than rare earth (RE) ions (e.g, Er^{3+}). The use of sensitizers, e.g., Cr^{3+}, Yb^{3+}, Bi^{3+},[8-10] which have much larger energy harvesting of pump light sources, is an effective strategy to improve the emission gains of Ni^{2+}. For example, the integrated emission intensity of Ni^{2+} has been enhanced by a factor of 4.4 (4.0) as a result of energy transfer (ET) from Yb^{3+} (Bi^{3+}) to Ni^{2+} at the 980 nm excitation. It is of practical value that the sensitization can be realized using a 980 nm InGaAs laser diode (LD) which is commercially available. According to Dexter's formula,[6] a significant spectral overlap is required to achieve an optimal sensitization effect, between the absorption of the activator (Ni^{2+}) and the emission of the sensitizer (Cr^{3+}, Yb^{3+}, Bi^{3+}). It is surprising to note that Nd^{3+}, a "superstar" dopant strongly lasing within the wavelength region similar to Yb^{3+} (1000-1100 nm),[11] has not yet been investigated as a possible sensitizer for Ni^{2+}.

A clear advantage of using Nd^{3+} as the sensitizer is related to the fact that it has a very high absorption cross-section at ~ 800 nm, and thus can be efficiently pumped by low-cost and high-power AlGaAs LDs. Moreover, the fact that Nd^{3+} possesses many excited states makes it

possible to be excited at a great variety of wavelengths from ultraviolet (UV) to visible. Nd^{3+} has been widely used as the sensitizer for a number of mid-infrared (MIR) and NIR-emitting ions such as Yb^{3+}, Er^{3+} and Ho^{3+} etc..[12-14] For example, the very efficient ET of Nd^{3+} → Yb^{3+} has been utilized for the development of a broadband high power fiber laser[12] and improving solar cell efficiency.[15] Additionally, since water has a much weaker (by a factor of 20) absorption at ~ 800 nm compared to 980 nm, much attention has been given of Nd^{3+} → Yb^{3+} for the enhanced emission in the second "biological window" (1000-1350 nm).[16] To overcome the limited ET efficiency of Nd^{3+} → Ho^{3+} due to the large energy mismatch, an ET bridge model has been proposed utilizing Nd^{3+} → Yb^{3+} → Ho^{3+}, where Yb^{3+} was used as an ET intermediate resulting in the significantly enhanced upconversion and 2.0 μm emissions of Ho^{3+}.[17-18] Regarding the highly efficient Nd^{3+} → Yb^{3+} and Yb^{3+} → Ni^{2+} processes, it is of great interest to establish whether Yb^{3+} could play a similar bridging role in the process of Nd^{3+} → Yb^{3+} → Ni^{2+}.

In this article, the sensitization effect of Nd^{3+} on Ni^{2+} is reported for the first time and the ET bridging role of Yb^{3+} is illustrated. Finally, the promising $Nd^{3+}/Yb^{3+}/Ni^{2+}$ doping scheme has led to the use of dual-laser pumping as a highly efficient means of generating the greatest enhancement of Ni^{2+} emissions in nano-GCs reported to date.

2. Experiment

Glass samples with the nominal compositions of (in mol %) $64SiO_2$-$23Ga_2O_3$-$13Li_2O$-xNd_2O_3-yYb_2O_3-$zNiO$ (x = 0, 0.3, y = 0.1, 0.3, 0.5, 0.7, 1.0, z = 0, 0.15) were prepared by the conventional melt quenching method. The raw materials were high purity

(4N) SiO_2, Ga_2O_3, Li_2O, NiO, Nd_2O_3 and Yb_2O_3 compounds. 30 g of the raw materials was mixed completely and melted in a quartz crucible at 1650°C for 1 hour in air. The melt was cast onto a copper plate, and then annealed at 550°C for 3 hours, forming the precursor glasses (PGs). The PGs were subsequently heated at 740°C for 5hours to obtain the transparent nano-GCs.

X-ray diffraction (XRD) was performed on the powder samples. The diffraction patterns were recorded using an X-ray diffractometer (D/MAX2550VB/PC, Rigaku Corporation, Japan) with Cu-Kα irradiation. A Scanning TEM (STEM) and high angle annular dark field STEM (HAADF-STEM) were used to analyze the current specimen using FEI Talos F200x, USA, operating at 200 kV and ~ 50 pA and was also equipped with an energy-dispersive spectrometer (EDS) system. The TEM examination was performed very carefully such that no noticeable damages was apparent to the samples during measurement. Further detailed explanation of the TEM measurement and sample preparation, are included in recent publications including authors of this article.[5-8]

Photoluminescence emission, PL decay and time-resolved emission spectra (TRES) were recorded using an FLS980 fluorescence spectrometer (Edinburgh Instruments) equipped with the single photon counting technique. The emission spectra were corrected using the instrumental response. For the TRES measurement, a series of PL decay curves were recorded in the wavelength range from 850 to 1700 nm at a 2 nm interval, and the TRES were obtained by slicing the recorded PL decay curves.[19] The lifetime resolution is 5 μs.

3. Results and discussion

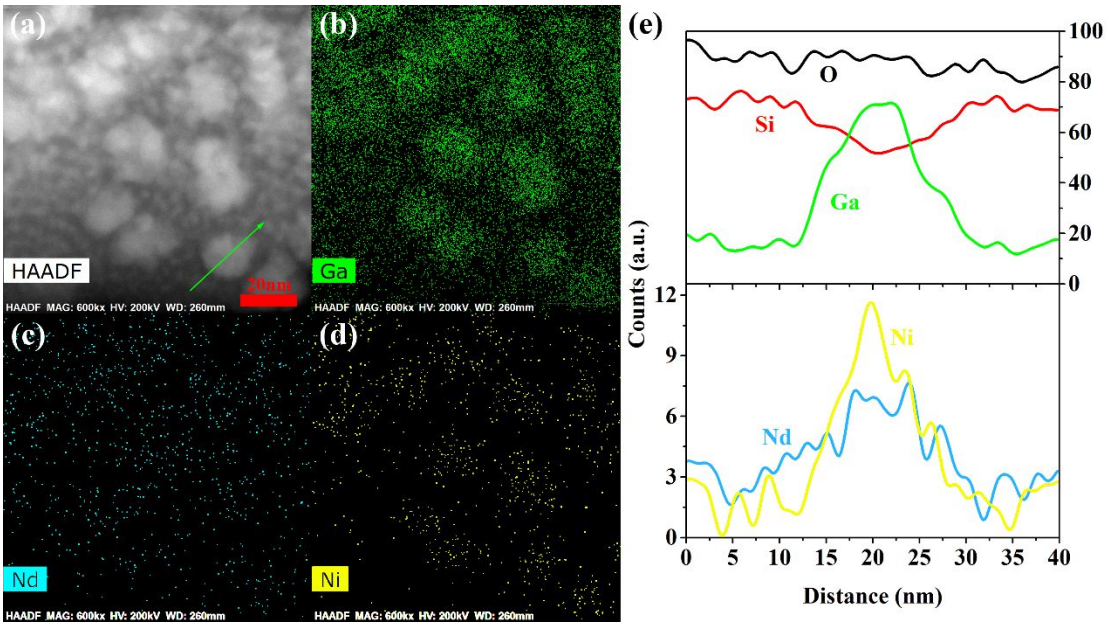

Figure 1. A typical HAADF-STEM image of the (in mol %) 2.0 Nd^{3+}/1.0 Ni^{2+} codoped nano-GCs (a), and the corresponding STEM-EDS mappings for Ga (b), Nd (c) and Ni (d) elements with their relative concentrations reflected by the brightness in colors. (e) The linescan analyses for the elements.

Upon thermal treatment of the PG samples, γ-Ga_2O_3 NCs with a particle size of approximately 20 nm were formed according to XRD and TEM measurements (Fig. S1, supporting information). STEM-EDS was used to identify the distribution of the dopants in the nano-GCs (Fig. 1). According to our recent quantitative characterizations, more than 90% of the doped Ni^{2+} ions were accumulated in the thermally grown Ga_2O_3 NCs, whereas the degree to which extent the RE ions were enriched in the Ga_2O_3 NCs depended on the ionic size of the RE ions, viz., the

doping efficiency of RE ions in Ga_2O_3 NCs decreases with increasing ionic radius, e.g., 76 % Yb^{3+} versus 55% Nd^{3+}.[5-6] Because of the smaller doping efficiency of Nd^{3+} as compared to Ni^{2+} in the Ga_2O_3 NCs, the enrichment of Nd^{3+} in the Ga_2O_3 NCs as reflected by the brightness in color of Fig. 1(c) is not very sharp. As such, to unambiguously confirm the enrichment of Nd^{3+} in the Ga_2O_3 NCs, the STEM-EDS linescan analysis was employed as shown in Fig. 1(e). The results are in accordance with previous studies.[5-6]

The nano-GCs are highly transparent as illustrated in the inset in Fig. 2. The absorption bands centered at 436, 855 and 1730 nm in the PG sample are ascribed to the fivefold coordinated Ni^{2+}.[1, 20-21] They convert to 381, 626 and 1050 nm in the nano-GCs, which can be attributed to the spin-allowed $^3A_2(F) \rightarrow {}^3T_1(P)$, $^3A_2(F) \rightarrow {}^3T_1(F)$ and $^3A_2(F) \rightarrow {}^3T_2(F)$ transitions of Ni^{2+} in octahedral sites.[7] By fitting the absorption bands of Ni^{2+} to the Tanabe-Sugano (TS) diagram for an d^8 ion, the values of Racah parameter (B) and crystal field strength (Dq) were obtained equal to 887 and 981 cm^{-1}, very close to the values reported by Zhou et al in Ni^{2+} doped β-Ga_2O_3 NCs.[21] The sharp absorption bands centered at 511, 524, 582, 681, 747, 805, 880 nm are due to the transitions from the $^4I_{9/2}$ ground state to the $^4G_{9/2}$, $^4G_{7/2}$, ($^4G_{5/2}$, $^2G_{7/2}$), $^4F_{9/2}$, ($^4F_{7/2}$, $^4S_{3/2}$), ($^4F_{5/2}$, $^2H_{9/2}$), and $^4F_{3/2}$ excited states of Nd^{3+}. The strong absorption band at 976 nm is attributed to the $^2F_{7/2} \rightarrow {}^2F_{5/2}$ transition of Yb^{3+}.[7, 22] From an energy matching point of view, the $^3T_2(F)$ excited state of Ni^{2+} centered at 1050 nm (9524 cm^{-1}) is energetically more favorable in resonant with the $^2F_{5/2}$ state of Yb^{3+} (10246 cm^{-1}) than with the $^4F_{3/2}$ state of Nd^{3+} (11364 cm^{-1}). This may

account for the fact that the ET efficiency of Yb^{3+} → Ni^{2+} is much larger than that of Nd^{3+} → $Ni^{2+}$and is discussed in the following section.

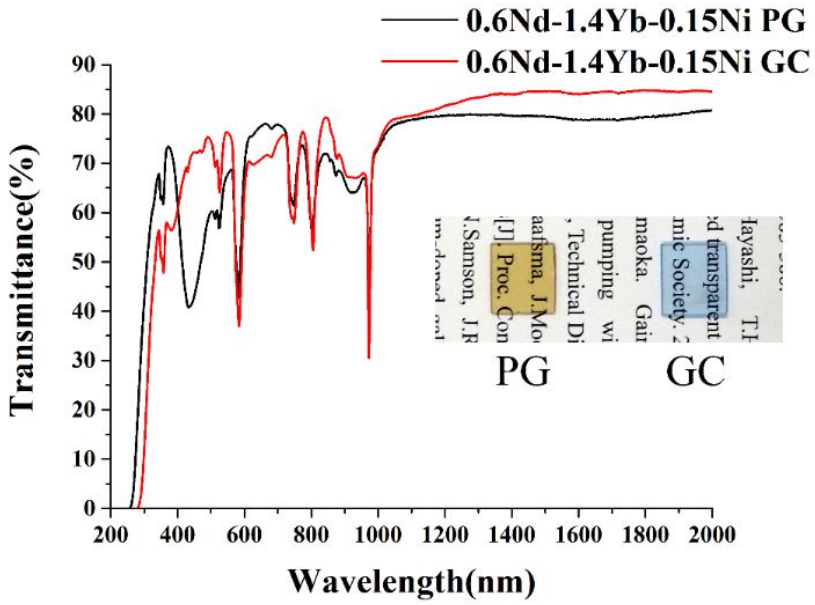

Figure 2. Transmission spectra of the (in mol %) 0.6 Nd^{3+}/1.4 Yb^{3+}/0.15 Ni^{2+} triply doped precursor glass (PG) and nano-glass ceramic (GC) samples. The inset shows the digital photographs of the corresponding samples.

Emission spectra are compared for the Nd^{3+}/Ni^{2+} codoped, Nd^{3+}- and Ni^{2+}-singly doped nano-GC samples as shown in Fig. 3(a). No NIR emission was observed from the Ni^{2+}-singly doped sample when excited using the 808 nm pump source, whereas the sample containing only Nd^{3+} exhibited three emission bands peaking at ~ 880, 1058 and 1333 nm, which are due to the $^4F_{3/2}$ → $^4I_{9/2}$, $^4F_{3/2}$ → $^4I_{11/2}$ and $^4F_{3/2}$ → $^4I_{13/2}$ transitions, respectively. In the Nd^{3+}/Ni^{2+} codoped sample, an ultra-broad Ni^{2+} emission band appears at ~ 1300 nm due to the $^3T_2(F)$ → $^3A_2(F)$ transition while the intensities of the emission bands related to an Nd^{3+} decrease. The results

clearly indicate that there exists an ET from Nd^{3+} to Ni^{2+}. The simultaneous weakening of all the three emission bands of Nd^{3+} suggests a nonradiative ET mechanism of Nd^{3+} → Ni^{2+}. This was further confirmed by PL lifetime measurement. As shown in Fig. 3(b), the lifetime of the $^4F_{3/2}$ excited state of Nd^{3+} is slightly reduced in the codoped sample as compared with that of the singly doped one. The efficiency of Nd^{3+} → Ni^{2+} is only 34.8% according to $\eta_{ET} = (1 - \tau/\tau_0)\times 100$ %, where τ and τ_0 are the lifetimes of Nd^{3+} in the presence and absence of Ni^{2+}, respectively. Note that the doping concentration of Nd^{3+} was optimized, otherwise concentration quenching would occurs when the Nd^{3+} content was over 0.6 mol.% as shown in the supporting information (Fig. S2). Although the ET efficiency was not very high in the present case, there is room for further improvement, this is because: in contrast to RE ions, the electronic transitions of Ni^{2+} are extremely sensitive to ligand fields, thus can be tuned in favor of a much stronger energy resonance and ET between the excited states of Ni^{2+} and Nd^{3+}.[1]

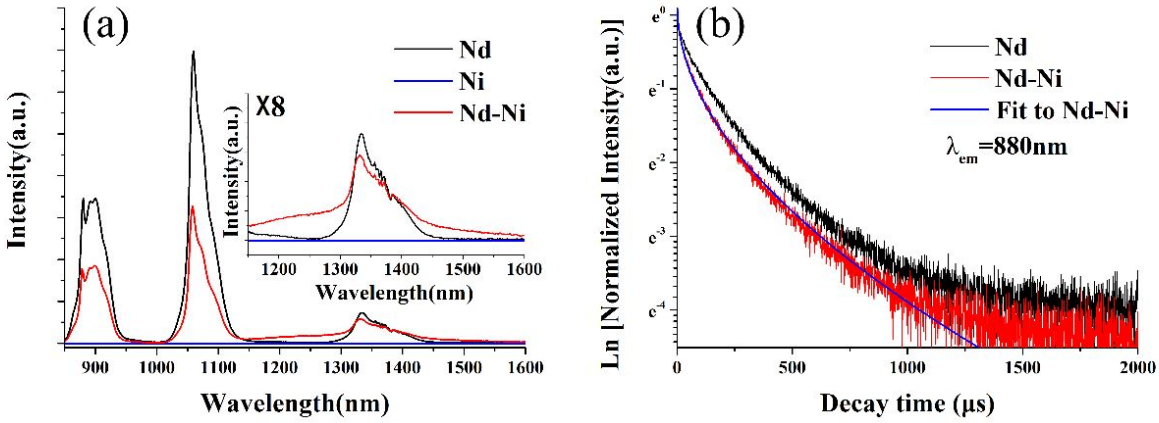

Figure 3. (a) Emission spectra of the (in mol %) 0.6 Nd^{3+} singly, 0.15 Ni^{2+} singly and 0.6 Nd^{3+}/0.15 Ni^{2+} codoped nano-glass ceramic samples at the 808 nm excitation. The inset enlarges

the specified wavelength region by 8 times. (b) PL decay curves of Nd^{3+} in the codoped and singly doped samples, and the fit (blue curve) to the experimental data.

The interaction mechanism between Nd^{3+} and Ni^{2+} can be extracted by fitting the normalized decay curve of the codoped sample against the Inokuti-Hirayama function as: $I = I_0 \exp(-\gamma t - Ct^{3/n})$, where I_0 is the non-decayed intensity, t is time, γ and C are fitting parameters, and n = 6, 8, 10 for electric-dipole-dipole, dipole-quadrupole, quadrupole-quadrupole interactions, respectively.[23] A good quality of fitting, R^2 = 0.996, was achieved for n = 6 indicative of an electric-dipole interaction. According to Blasse,[24] the critical distance of interaction, Rc (Å), can be calculated using the expression, $R_c^6 = 2.88\times10^{12} f_A E^{-4} \int g_D g_A dE$ where E is the energy of the maximum spectral overlap between the emission spectrum of Nd^{3+} (g_D) and the absorption spectrum of Ni^{2+} (g_A) both normalized in a sense that $\int g_D(E)dE = \int g_A(E)dE = 1$, and f_A is the absorption cross-section at wavelength λ (nm) obtained by: $0.113/\lambda^2 \times \int \sigma(\lambda) d\lambda$ where $\sigma(\lambda)$ is) is the oscillator strength of Ni^{2+}. The critical distance obtained using this method was ~ 8.4 Å. Such a short distance can be realized only if both Nd^{3+} and Ni^{2+} are accumulated in the γ-Ga_2O_3 NCs precipitated in the GCs, which conforms to the STEM results shown in Fig. 1. The calculated microscopic ET parameter ($C_{DA} = R_c^6 \tau_0^{-1}$, where τ_0 is the intrinsic lifetime of donor) is 21.7 $\times10^{-40}$ $cm^6 \bullet s^{-1}$ as listed in Table 1.

The sensitization of Ni^{2+} by Nd^{3+} has been successfully demonstrated and reported for the first time. However, due to limited efficiency (34.8 %), only a rather weak emission of Ni^{2+} was obtained. This is in sharp contrast to the case of sensitization by Yb^{3+}. For example, it was

recently reported by some of the authors of this article that the efficiency of $Yb^{3+} \rightarrow Ni^{2+}$ can be as high as ~ 70 % in the identical nano-GCs.[7-8] The discrepancy arises mainly because of the larger energy mismatch in $Nd^{3+} \rightarrow Ni^{2+}$ (~ 1840 cm^{-1}) than in $Yb^{3+} \rightarrow Ni^{2+}$ (~ 722 cm^{-1}). According to the Raman spectra (Fig. S4, supporting information), the largest phonon energies of the glass matrix and γ-Ga_2O_3 NCs are approximately 1000 and 760 cm^{-1}, respectively. This means that the ET of $Nd^{3+} \rightarrow Ni^{2+}$ is assisted by at least two phonons while only one phonon is required in $Yb^{3+} \rightarrow Ni^{2+}$. The efficiency of the phonon-assisted ET scales inversely with the number of phonons involved.[25] The $Yb^{3+} \rightarrow Ni^{2+}$ involving only one phonon is therefore expected to be much more efficient than $Nd^{3+} \rightarrow Ni^{2+}$. The microscopic ET parameter of $Yb^{3+} \rightarrow Ni^{2+}$ is nearly three times of that of $Nd^{3+} \rightarrow Ni^{2+}$ (Table 1). Likewise, $Nd^{3+} \rightarrow Yb^{3+}$ with the participation of only one phonon is very efficient when used in high phonon energy glasses.[26] The efficiency can be as high as 53.6 % in the nano-GCs of this investigation (Table 1). A detailed analysis of the ET mechanism of $Nd^{3+} \rightarrow Yb^{3+}$ can be found in the supporting information (Fig. S5).

Since the energy level of Yb^{3+} lies midway between those of Nd^{3+} and Ni^{2+} (Fig. 5), employing Yb^{3+} as the ET intermediate or bridge therefore provides a rational solution to boosting the overall efficiency of $Nd^{3+} \rightarrow Ni^{2+}$.[18] As shown in Fig. 4(a), the addition of Yb^{3+} significantly enhances the emission of Ni^{2+}. As the concentration of Yb^{3+} increases, the emission intensity of Nd^{3+} decreases whereas that of Ni^{2+} increases. Because the broad emission band contains the contributions from both the emissions of Ni^{2+} (centered at 1270 nm) and Nd^{3+} (centered at 1335

nm), the overall lineshape in the range of 1150 to 1600 nm varies with the doping concentration of Yb^{3+}. When the concentration of Yb^{3+} reaches 1.4 mol %, the emission intensity of Ni^{2+} was observed to be larger (by more than three times) than that of the Nd^{3+}/Ni^{2+} codoped sample free of Yb^{3+}. The Ni^{2+} emission decreases with further increasing content of Yb^{3+} due to concentration quenching of the Yb^{3+} emission (Fig. S3, supporting information). The lifetime of Yb^{3+} evidently reduces in the triply doped sample as compared with the codoped case free of Ni^{2+} [Fig. 4(b)], suggesting a non-radiative ET of $Yb^{3+} \rightarrow Ni^{2+}$ with an efficiency of 79.3 %. The internal quantum efficiency of the Ni^{2+} emission is 62.5 % (Fig. S6, supporting information), which is much higher than that of the $ZnGa_2O_4$: Ni^{2+} nano-GCs (25 %).[20] The result of the normalized decay curve (Fig. 4b) of the triply doped sample shows that $Yb^{3+} \rightarrow Ni^{2+}$ occurs via electric-dipole interactions. The critical distance of interaction between Yb^{3+} and Ni^{2+} is ~ 13.2 Å (Table 1). Again the efficient ET of $Yb^{3+} \rightarrow Ni^{2+}$ is only possible if the dopants are both accumulated in the thermally grown NCs in the GCs.[5-6]

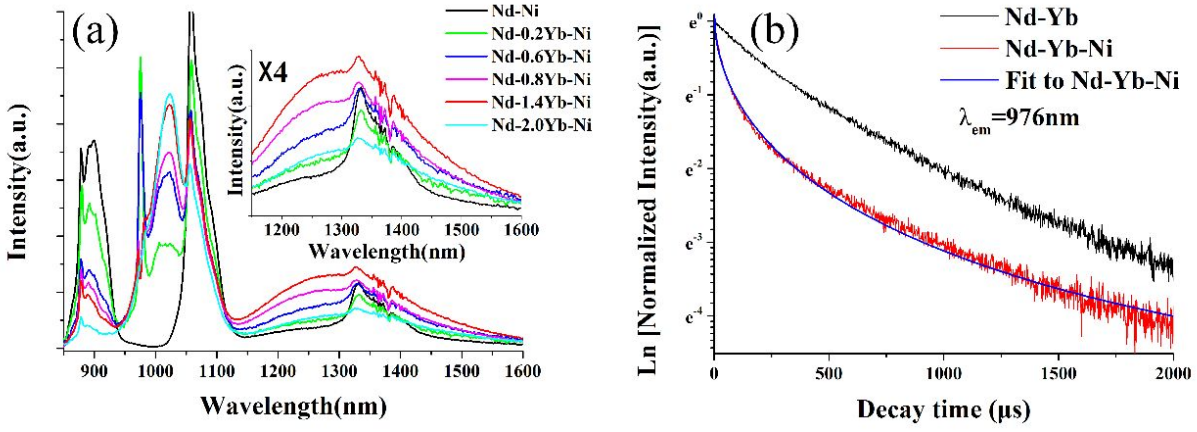

Figure 4. (a) Emission spectra of the (in mol %) 0.6 Nd^{3+}/*x* Yb^{3+} (*x* = 0, 0.2, 0.6, 1.0, 1.4, 2) /0.15 Ni^{2+} triply doped nano-glass ceramic samples at the 808 nm excitation. The inset enlarges the specified wavelength region by 4 times. (b) PL decay curves of Yb^{3+} in the 0.6 Nd^{3+}/1.4 Yb^{3+} codoped and 0.6 Nd^{3+}/1.4 Yb^{3+}/0.15 Ni^{2+} triply doped samples, and the fit (blue curve) to the experimental data.

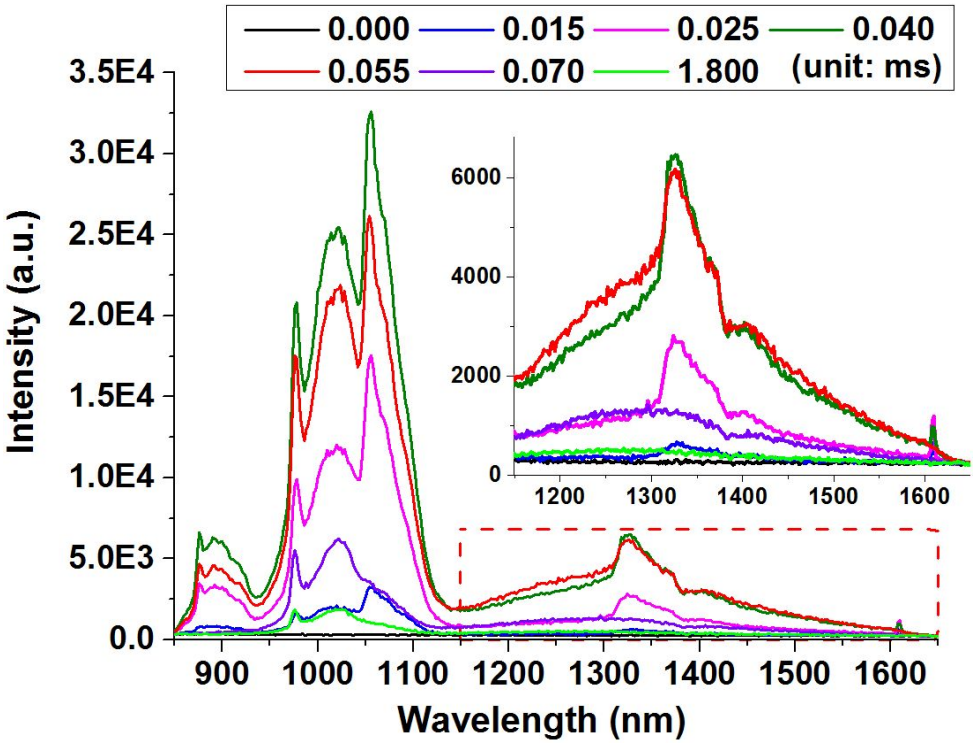

Figure 5. Time-resolved emission spectra of the (in mol %) 0.6 Nd^{3+}/1.4 Yb^{3+}/0.15 Ni^{2+} triply-doped nano-glass ceramic (GC). Inset: expanded spectra in the range of 1150 to 1650 nm.

The ET processes between the dopants can be straightforwardly understood by means of time-resolved emission spectra (TRES) as shown in Fig. 5. When excited by a pulsed 808 nm LD, initially only the emissions of Nd^{3+} and Yb^{3+} could be simultaneously recorded in the first 15 μs. Noticeable Ni^{2+} emission was observed 10 μs later. The Nd^{3+} and Yb^{3+} emissions kept

increasing until 40 μs, but the strongest Ni^{2+} emission was achieved about 15 μs later. In other words, the Nd^{3+} and Yb^{3+} emissions had already decayed before a Ni^{2+} reached its maximum emission. After another 10 μs, the Nd^{3+} emission totally disappeared such that Yb^{3+} and Ni^{2+} emissions were left behind. In the end, only the Yb^{3+} emission persisted 1.8 ms after the excitation and the Ni^{2+} emission was too weak to be detected. The coexistence of the Nd^{3+} and Yb^{3+} emissions in the very beginning of the excitation suggests an extremely fast $Nd^{3+} \rightarrow Yb^{3+}$ process, which is in a sub-microsecond regime limited by the resolution of the TRES measurement. The fact that Ni^{2+} emits lagging behind Nd^{3+} and Yb^{3+} reflects efficient ET from Nd^{3+} and Yb^{3+} to Ni^{2+}. Moreover, the fact that the Ni^{2+} keeps emitting (at 0.07 ms) even when the Nd^{3+} emission totally fades away substantiates the important role of Yb^{3+} on the enhancement of the Ni^{2+} emission.

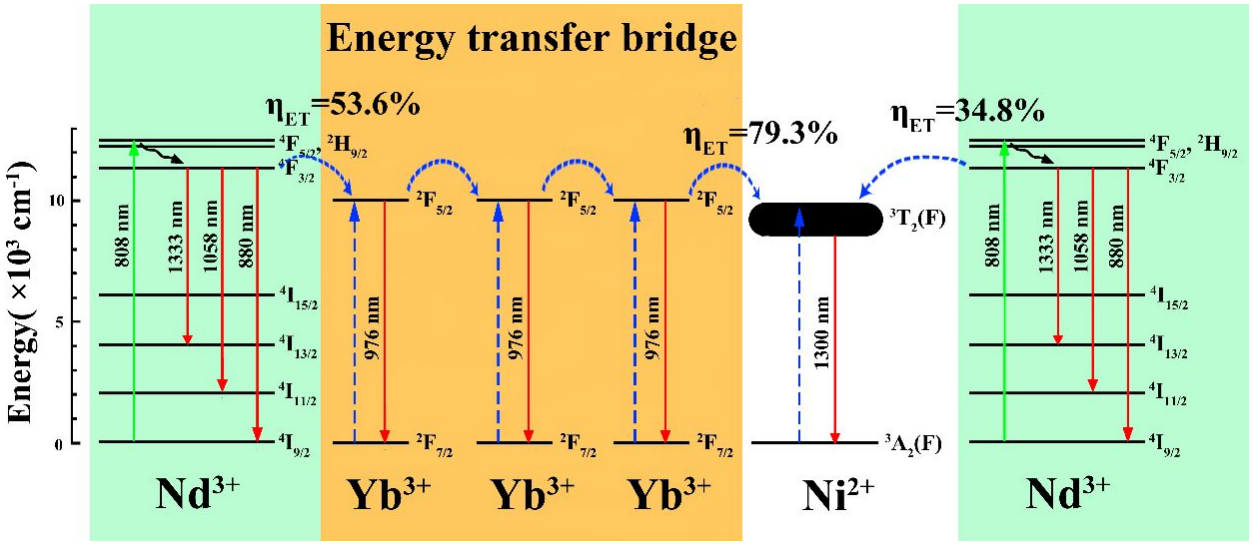

Figure 6. Energy level diagrams of Nd^{3+}, Yb^{3+}, Ni^{2+} and the involved ET processes among the dopants in the studied GCs.

Based on the above results, the ET interactions between Nd^{3+}, Yb^{3+} and Ni^{2+} are schematically illustrated in Fig. 6. Clearly, the addition of Yb^{3+} specifically providing the ET bridging, a better energy level matching scheme is obtained with a much increased ET efficiency. The stimulated emission cross section (σ_e) calculated using the McCumber formula [3] is 0.75 × 10^{-20} cm^2. The product of σ_e and τ_{300K} (proportional to the amplification gain) taken as a figure of merit (FOM)[27] is then 3.78 × 10^{-24} cm^2•s, which is much larger than that of $ZnGa_2O_4$: Ni^{2+} (1.23 × 10^{-24} cm^2•s) and comparable to that of $LiGa_5O_8$: Ni^{2+} (~ 3.70 × 10^{-24} cm^2•s) nano-GCs.[20]

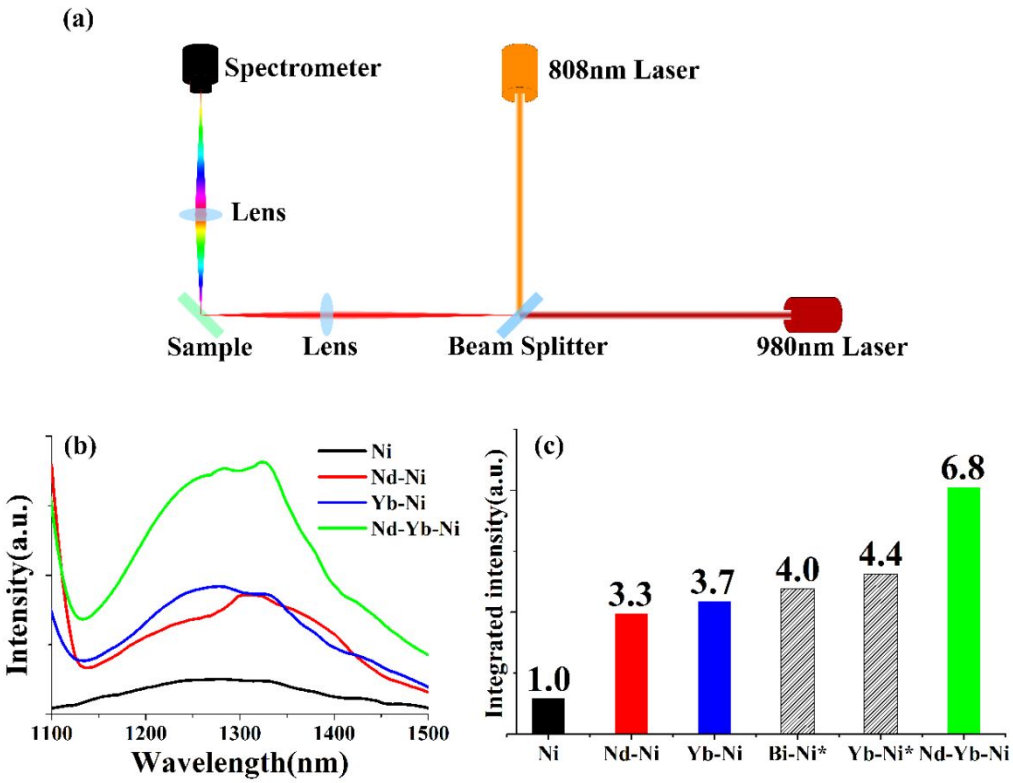

Figure 7. (a) Setup for PL measurement by the dual-laser pumping scheme. (b) Emission spectra of the Ni^{2+} singly, Nd^{3+}/Ni^{2+}, Yb^{3+}/Ni^{2+} codoped, and $Nd^{3+}/Yb^{3+}/Ni^{2+}$ triply doped nano-GCs under the same pumping conditions. (c) Comparision of enhancement factor (indicated by the

numbers) of Ni^{2+} emission in various nano-GCs. The factor is normalized with respect to the integrated emission intensity of the Ni^{2+} singly doped sample. The contribution of the Nd^{3+} emission was subtracted in calculating the integrated emission intensity. The stars represent data taken from Refs. 10 and 22.

The novel $Nd^{3+}/Yb^{3+}/Ni^{2+}$ doping, combining both the advantages of Nd^{3+} and Yb^{3+}, provides incentive to further investigate the effect of simultaneously dual-laser pumping at 808 and 980 nm on the Ni^{2+} Emission. Although such a dual-laser pumping scheme has recently been shown to be of benefit for achieving broad gain in a Nd^{3+}/Yb^{3+} codoped silica glass fiber amplifier,[12] to the best of knowledge of the authors it has not been utilized for Ni^{2+} to date. The experimental setup for the dual-laser pumping is shown in Fig. 7(a). Under the fixed pumping conditions (e.g., laser output powers and sample arrangement), the strongest emission of Ni^{2+} was found in the $Nd^{3+}/Yb^{3+}/Ni^{2+}$ triply doped sample as compared with the Ni^{2+} singly, Nd^{3+}/Ni^{2+} and Yb^{3+}/Ni^{2+} codoped samples [Fig. 7(b)]. A quantitative comparison of the integrated emission intensity of Ni^{2+} is shown in Fig. 7(c). Note that because the emission band from 1100 to 1500 nm contains contributions from both the Ni^{2+} and Nd^{3+} emission, the latter was subtracted in calculating the integrated emission intensities.

Thanks to the co-sensitization effect of Nd^{3+} and Yb^{3+}, a seven-fold enhancement is achieved in the triply doped sample, which is the largest value reported to date in Ni^{2+} doped GCs.[10, 22] To understand such effect, we have compared the emission spectra of the $Ni^{2+}/Yb^{3+}/Nd^{3+}$ system

optical amplification has been previously demonstrated at 1300 nm in a Ni^{2+} singly doped nano-GC containing Ga_2O_3 NCs.[21] Considering the much larger FOM and enhancement of Ni^{2+} emission achieved with the nano-GCs studied in this investigation, a further improvement in optical gain is expected. Furthermore, these nano-GCs have been recently shown to be capable of drawing into optical fibers using a melt-in-tube method.[28] Future work will include a detailed study of the optical amplification using optical fibers based on the $Nd^{3+}/Yb^{3+}/Ni^{2+}$ triply doped nano-GCs.

Table 1. The ET efficiency (η_{ET}), critical distance (Rc) and microscopic parameter (C_{DA}) between the donor (D) and the acceptor (A) in samples.

D → A	Transitions	η_{ET}	Rc (Å)	C_{DA} ($\times 10^{-40}$ cm^6•s^{-1})
Nd^{3+} → Ni^{2+}	$^4F_{3/2}$ → $^3T_2(F)$	34.8%	8.4	21.7
Nd^{3+} → Yb^{3+}	$^4F_{3/2}$ → $^2F_{5/2}$	53.6%	18.2	98.1
Yb^{3+} → Ni^{2+}	$^2F_{5/2}$ → $^3T_2(F)$	79.3%	13.2	59.1

4. Conclusion

All the dopants appear to be preferentially accumulated in the γ-Ga_2O_3 NCs thermally grown in the nano-GCs. An enhanced broadband NIR emission of Ni^{2+} has been successfully obtained when excitation of Nd^{3+} was provided from an 808 nm laser diode source. The overall ET efficiency was enhanced with the addition of Yb^{3+} as the ET bridge. The important role of Yb^{3+} on the enhancement of the Ni^{2+} emission has been substantiated. Based on the theoretical

calculations, the following conclusions can be drawn: a) the Nd^{3+} → Ni^{2+}, Nd^{3+} → Yb^{3+} and Yb^{3+} → Ni^{2+} all occur via the electric-dipole interactions, and b) the Nd^{3+} → Ni^{2+} and Yb^{3+} → Ni^{2+} can be efficient only if the donor and acceptor are in close proximity to each other. Using the dual-laser pumping scheme, the largest enhancement was achieved of the Ni^{2+} emission reported to date. The $Nd^{3+}/Yb^{3+}/Ni^{2+}$ triply doped nano-GCs with a much larger FOM are a highly promising gain medium for broadband and tunable fiber amplifiers. Moreover, the novel Nd^{3+} → Yb^{3+} → Ni^{2+} ET strategy demonstrated in this article can be extended to a broad range of nano-material systems (e.g., $KZnF_3$), which are capable of converting the 808 nm NIR light to within the second biological window, and thus is of significant interest to researchers studying in the field of bioimaging and related areas.

Supporting Information

Analysis of XRD patterns, bright field TEM image, selected area electron diffraction pattern, HRTEM image, the emission spectra of Nd^{3+}, the emission spectra of Yb^{3+}, Raman spectra, the energy transfer of Nd^{3+} → Yb^{3+} and the internal quantum efficiency of the samples.

Acknowledgments

This study was supported by the National Natural Science Foundation of China (51872055, 61775045, 61805054, 61850410537, 61605030), Natural Science Foundation of Heilongjiang Province of China (F2017006), the Fundamental Research Funds for the Central Universities and the 111 project (B13015) to the Harbin Engineering University.

References

1. Zhou, S.; Jiang, N.; Wu, B.; Hao, J.; Qiu, J. Ligand-driven wavelength-tunable and ultra-broadband infrared luminescence in single-ion-doped transparent hybrid materials. *Adv. Funct. Mater.* **2009,** *19* (13), 2081-2088.

2. Hughes, M.; Rutt, H.; Hewak, D.; Curry, R. J. Spectroscopy of vanadium (III) doped gallium lanthanum sulphide chalcogenide glass. *Appl. Phys. Lett.* **2007,** *90* (3), 031108.

3. Ren, J.; Li, B.; Yang, G.; Xu, W.; Zhang, Z.; Secu, M.; Bercu, V.; Zeng, H.; Chen, G. Broadband near-infrared emission of chromium-doped sulfide glass-ceramics containing Ga_2S_3 nanocrystals. *Opt. Lett.* **2012,** *37* (24), 5043-5045.

4. Miyata, T.; Nakatani, T.; Minami, T. Gallium oxide as host material for multicolor emitting phosphors. *J. Lumin.* **2000,** *87-89*, 1183-1185.

5. Gao, Z.; Lu, X.; Chu, Y.; Guo, S.; Liu, L.; Liu, Y.; Sun, S.; Ren, J.; Yang, J. The distribution of rare earth ions in a γ-Ga_2O_3 nanocrystal-silicate glass composite and its influence on the photoluminescence properties. *J. Mater. Chem. C* **2018,** *6* (12), 2944-2950.

6. Gao, Z.; Guo, S.; Lu, X.; Orava, J.; Wagner, T.; Zheng, L.; Liu, Y.; Sun, S.; He, F.; Yang, P. et al. Controlling selective doping and energy transfer between transition metal and rare earth ions in nanostructured glassy solids. *Adv. Opt. Mater.* **2018,** *6* (13), 1701407.

7. Gao, Z.; Lu, X.; Zhang, Y.; Guo, S.; Liu, Y.; Sun, S.; He, F.; Yang, P.; Ren, J.; Yang, J. Transmission electron microscopic and optical spectroscopic studies of $Ni^{2+}/Yb^{3+}/Er^{3+}/Tm^{3+}$ doped dual-phase glass-ceramics. *J. Am. Ceram. Soc.* **2018,** *101* (7), 2868-2876.

8. Gao, Z.; Lu, X.; Zhang, Y.; Guo, S.; Liu, L.; Yang, G.; Liu, Y.; Sun, S.; Ren, J.; Yang, J. Correlation between ultrabroadband near-infrared emission and Yb^{3+}/Ni^{2+} dopants distribution in highly transparent germanate glass ceramics containing zinc gallogermanate nanospinels. *J. Am. Ceram. Soc.* **2018,** *10.1111*, jace.16028.

9. Wu, B.; Zhou, S.; Ruan, J.; Qiao, Y.; Chen, D.; Zhu, C.; Qiu, J. Energy transfer between Cr^{3+} and Ni^{2+} in transparent silicate glass ceramics containing Cr^{3+}/Ni^{2+} co-doped $ZnAl_2O_4$ nanocrystals. *Opt. Express* **2008,** *16* (4), 2508-2513.

10. Zhang, K.; Zhou, S.; Zhuang, Y.; Yang, R.; Qiu, J. Bandwidth broadening of near-infrared emission through nanocrystallization in Bi/Ni co-doped glass. *Opt. Express* **2012,** *20* (8), 8675-8680.

11. Holzrichter, J. F. High-power solid-state lasers. *Nature* **1985,** *316*, 309.

12. Lin, Z.; Wang, F.; Wang, M.; Zhang, L.; Feng, S.; Gao, G.; Wang, S.; Yu, C.; Hu, L. Maintaining broadband gain in a Nd^{3+}/Yb^{3+}co-doped silica fiber amplifier via dual-laser pumping. *Opt. Lett.* **2018,** *43* (14), 3361-3364.

13. Zhang, P.; Wang, R.; Huang, X.; Li, Z.; Yin, H.; Zhu, S.; Chen, Z.; Hang, Y. Sensitization and deactivation effects to Er^{3+} at ~2.7 μm mid-infrared emission by Nd^{3+} ions in $Gd_{0.1}Y_{0.9}AlO_3$ crystal. *J. Alloys Compd.* **2018,** *750*, 147-152.

14. Li, L. X.; Wang, W. C.; Zhang, C. F.; Yuan, J.; Zhou, B.; Zhang, Q. Y. 2.0 μm Nd^{3+}/Ho^{3+}-doped tungsten tellurite fiber laser. *Opt. Mater. Express* **2016,** *6* (9), 2904-2914.

15. Costa, F. B.; Yukimitu, K.; Nunes, L. A. d. O.; Figueiredo, M. d. S.; Silva, J. R.; Andrade, L. H. d. C.; Lima, S. M.; Moraes, J. C. S. High $Nd^{3+} \rightarrow Yb^{3+}$ energy transfer efficiency in tungsten-tellurite glass: A promising converter for solar cells. *J. Am. Ceram. Soc.* **2017,** *100* (5), 1956-1962.

16. Pedraza, F. J.; Rightsell, C.; Kumar, G. A.; Giuliani, J.; Monton, C.; Sardar, D. K. Emission enhancement through Nd^{3+}-Yb^{3+} energy transfer in multifunctional $NaGdF_4$ nanocrystals. *Appl. Phys. Lett.* **2017,** *110* (22), 223107.

17. Qiu, J.; Kawamoto, Y.; Zhang, J. Highly efficient green up-conversion luminescence of Nd^{3+}–Yb^{3+}–Ho^{3+} codoped fluorite-type nanocrystals in transparent glass ceramics. *J. Appl. Phys.* **2002,** *92* (9), 5163-5168.

18. Yuan, J.; Shen, S. X.; Wang, W. C.; Peng, M. Y.; Zhang, Q. Y.; Jiang, Z. H. Enhanced 2.0 μm emission from Ho^{3+} bridged by Yb^{3+} in $Nd^{3+}/Yb^{3+}/Ho^{3+}$ triply doped tungsten tellurite glasses for a diode-pump 2.0 μm laser. *J. Appl. Phys.* **2013,** *114* (13), 133506.

19. Chu, Y.; Hu, Q.; Zhang, Y.; Gao, Z.; Fang, Z.; Liu, L.; Yan, Q.; Liu, Y.; Sun, S.; Peng, G.-D. et al. Topological engineering of photoluminescence properties of bismuth- or erbium-doped phosphosilicate glass of arbitrary P_2O_5 to SiO_2 ratio. *Adv. Opt. Mater.* **2018,** *6* (13), 1800024.

20. Gao, Z.; Liu, Y.; Ren, J.; Fang, Z.; Lu, X.; Lewis, E.; Farrell, G.; Yang, J.; Wang, P. Selective doping of Ni^{2+} in highly transparent glass-ceramics containing nano-spinels $ZnGa_2O_4$ and $Zn_{1+x}Ga_{2-2x}Ge_xO_4$ for broadband near-infrared fiber amplifiers. *Sci. Rep.* **2017,** *7* (1), 1783.

21. Zhou, S.; Dong, H.; Feng, G.; Wu, B.; Zeng, H.; Qiu, J. Broadband optical amplification in silicate glass-ceramic containing β-Ga_2O_3:Ni^{2+} nanocrystals. *Opt. Express* **2007,** *15* (9), 5477-5481.

22. Wu, B.; Ruan, J.; Ren, J.; Chen, D.; Zhu, C.; Zhou, S.; Qiu, J. Enhanced broadband near-infrared luminescence in transparent silicate glass ceramics containing Yb^{3+} ions and Ni^{2+}-doped $LiGa_5O_8$ nanocrystals. *Appl. Phys. Lett.* **2008,** *92* (4), 041110.

23. Inokuti, M.; Hirayama, F. Influence of energy transfer by the exchange mechanism on donor luminescence. *J. Chem. Phys.* **1965,** *43* (6), 1978-1989.

24. Blasse, G. The physics of new luminescent materials. *Mater. Chem. Phys.* **1987,** *16* (3), 201-236.

25. Chu, Y.; Ren, J.; Zhang, J.; Peng, G.; Yang, J.; Wang, P.; Yuan, L. $Ce^{3+}/Yb^{3+}/Er^{3+}$ triply doped bismuth borosilicate glass: a potential fiber material for broadband near-infrared fiber amplifiers. *Sci. Rep.* **2016,** *6*, 33865.

26. Rivera-López, F.; Babu, P.; Basavapoornima, C.; Jayasankar, C. K.; Lavín, V. Efficient $Nd^{3+} \rightarrow Yb^{3+}$ energy transfer processes in high phonon energy phosphate glasses for 1.0 μm Yb^{3+} laser. *J. Appl. Phys.* **2011,** *109* (12), 123514.

27. Liu, Q.; Tian, Y.; Tang, W.; Huang, F.; Jing, X.; Zhang, J.; Xu, S. Broadening and enhancing 2.7μm emission spectra in Er/Ho co-doped oxyfluoride germanosilicate glass ceramics by imparting multiple local structures to rare earth ions. *Photon. Res.* **2018,** *6* (4), 339-345.

28. Fang, Z.; Zheng, S.; Peng, W.; Zhang, H.; Ma, Z.; Dong, G.; Zhou, S.; Chen, D.; Qiu, J. Ni^{2+} doped glass ceramic fiber fabricated by melt-in-tube method and successive heat treatment. *Opt. Express* **2015,** *23* (22), 28258-28263.

TOC Graphic

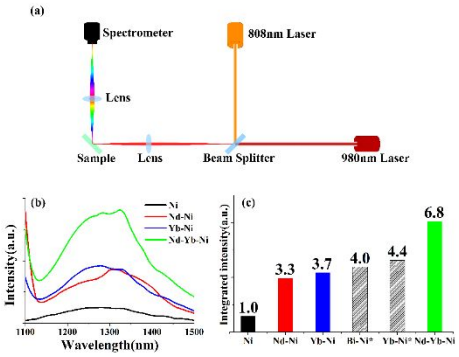
(a)
Spectrometer
808nm Laser
Lens
Sample
Lens
Beam Splitter
980nm Laser
(b)
Ni
Nd-Ni
Yb-Ni
Nd-Yb-Ni
Intensity(a.u.)
1100
1200
1300
1400
1500
Wavelength(nm)
(c)
Integrated intensity(a.u.)
1.0
3.3
3.7
4.0
4.4
6.8
Ni
Nd-Ni
Yb-Ni
Bi-Ni*
Yb-Ni*
Nd-Yb-Ni